Long-term cycling behavior of asymmetric activated carbon/MnO2 aqueous electrochemical supercapacitor

Thierry Brousse, Pierre-Louis. Taberna, Olivier Crosnier, Romain Dugas, Philippe Guillemet, Yves Scudeller, Frédéric Favier, Yingke K. Zhou, Daniel Bélanger, Patrice Simon

Long-term cycling behavior of asymmetric activated carbon/MnO_2 aqueous electrochemical supercapacitor

Thierry Brousse [a,*], Pierre-Louis Taberna [b], Olivier Crosnier [a], Romain Dugas [a], Philippe Guillemet [a], Yves Scudeller [a], Yingke Zhou [d], Frédéric Favier [d], Daniel Bélanger [c], Patrice Simon [b]

[a] *Laboratoire de Génie des Matériaux et Procédés Associés (LGMPA), Ecole polytechnique de l'Université de Nantes, Nantes Atlantique Université, rue Christian Pauc, BP50609, 44306 Nantes Cedex 3, France*

[b] *Centre Inter-universitaire de Recherche et d'Ingénierie des Matériaux (CIRIMAT, UMR 5085), Université Paul Sabatier, Bat 2 R1, 118 route de Narbonne, 31062 Toulouse Cedex 4, France*

[c] *Département de Chimie, Université du Québec à Montréal (UQAM), Case Postale 8888, succursale Centre-Ville, Montréal, Québec H3C 3P8, Canada*

[d] *Laboratoire des Aggrégats Moléculaires et Matériaux Inorganiques (LAMMI, UMR CNRS 5072) Université Montpellier II, cc015, 2 Place Eugène Bataillon, 34095 Montpellier Cedex 05, France*

Abstract

Activated carbon–MnO_2 hybrid electrochemical supercapacitor cells have been assembled and characterized in K_2SO_4 aqueous media. A laboratory cell achieved 195,000 cycles with stable performance. The maximal cell voltage was 2 V associated with $21 \pm 2\,F\,g^{-1}$ of total composite electrode materials (including activated carbon and MnO_2, binder and conductive additive) and an equivalent serie resistance (ESR) below $1.3\,\Omega\,cm^2$. Long-life cycling was achieved by removing dissolved oxygen from the electrolyte, which limits the corrosion of current collectors. Scaling up has been realized by assembling several electrodes in parallel to build a prismatic cell. A stable capacity of 380 F and a cell voltage of 2 V were maintained over 600 cycles. These encouraging results show the interest of developing such devices, including non-toxic and safer components as compared to the current organic-based devices.

Keywords: Supercapacitor; Electrochemical capacitor; Asymmetric device; MnO_2; Activated carbon

1. Introduction

Electrochemical capacitors [1–3], so-called supercapacitors, are intermediate devices between conventional dielectric capacitors and batteries. Nowadays, commercial devices are mainly based on two symmetric activated carbon electrodes [4–7] separated by a cellulosic or a polymeric membrane impregnated with an organic electrolyte, basically a salt, such as tetraethyl ammonium tetrafluoroborate dissolved in an organic solvent (acetonitrile or propylene carbonate). Such devices achieved long-term cycling behavior (several hundred thousand cycles) with impressive maximal power and energy densities of about $5\,kW\,kg^{-1}$ and $5\,Wh\,kg^{-1}$, respectively. However, their main drawback lies in the use of organic solvents, which can become hazardous in case of thermal runaway referring to a situation where an increase in temperature [8,9] changes the conditions in such way that it causes a further increase in temperature leading to a destructive result (vaporization of the solvent, inflammation, explosion of the supercapacitor). Additionally, the use of pure aprotic solvents leads to a detrimental cost of the electrolyte and of the overall fabrication process, which requires a water-free atmosphere. Alternative devices, using RuO_2 [10–13] or conducting polymers [14–16] as electrode materials, have not yet reached the performance of carbon/carbon supercapacitors in terms of energy and power densities, long-term cycling behavior and cost.

Recently, inexpensive transition-metal oxides, such as Fe_3O_4 [17–20] or MnO_2 [21–28], have been investigated as possible

* Corresponding author. Tel.: +33 2 40 68 31 73; fax: +33 2 40 68 31 99.
E-mail address: thierry.brousse@polytech.univ-nantes.fr (T. Brousse).

doi:10.1016/j.jpowsour.2007.04.074

supercapacitor electrode materials in mild aqueous electrolytes. Despite high specific capacitance, the cell voltage of symmetric devices is limited to 1 V [29], and subsequently both power and energy densities remain unsatisfactory for industrial applications. This fact led to the concept of asymmetric devices combining either two distinct oxide electrodes (Fe_3O_4 and MnO_2 [20,29]), an activated carbon electrode associated to an oxide electrode (MnO_2) [29–32], or a conducting polymer and an oxide electrode (MnO_2) [33], showing complementary active electrochemical windows in order to enhance the overall voltage of the resulting capacitor. Activated carbon/MnO_2 asymmetric device in aqueous K_2SO_4 is described in details in literature [29–32]. With such electrode materials, electrolyte and fabrication procedure, a very low cost device can be achieved as well as improved security versus thermal runaway. These asymmetric devices exhibit two different charge storage mechanisms. An electrochemical double layer capacitance (EDLC) rules the negative activated carbon electrode, while the manganese dioxide electrode shows a pseudo-capacitive behavior involving Mn^{III}/Mn^{IV} redox processes [34]. This difference in charge storage mechanisms enables us to refer to a so-called hybrid supercapacitor. In this study, "hybrid cell" or "asymmetric cell" [35] will be used indifferently, although it initially refers to two distinct concepts. It is related to the discrepancies in charge storage mechanisms between the positive and the negative electrodes (hybrid), but also to the distinct nature of active materials at the positive and negative electrode (asymmetric). Such a hybrid device (activated carbon as negative electrode and MnO_2 as positive) has been cycled between 0 and 2.2 V at constant power density (1.2 kW kg^{-1}) over 10,000 cycles [31]. However, in such voltage range, a constant fade in energy density is observed upon cycling, and only 55% of the initial energy density is retained after 10,000 cycles. Decreasing the maximum cell voltage to 1.5 V led to an improved stability, since 77% of the initial energy density is retained after 23,000 cycles [31]. However, by lowering the maximum cell voltage, both power and energy densities are decreased. At this point, it seems that the concept of carbon/MnO_2 asymmetric device in mild aqueous electrolyte could not reach the target of long-term cycling behavior as expected for supercapacitor applications (>100,000 cycles). Moreover, studies on MnO_2 supercapacitor electrodes usually comment on characteristics and performances over only a few thousand cycles, *de facto* highlighting the limitations of a pseudo-faradic electrode in an aqueous electrolyte for long-term use [29–33]. Additionally, manufacturing large capacitance devices (that can reach up to several hundred Farads) requires the use of several individual cells in parallel. Such cell build up is very common for activated carbon symmetric device in organic electrolyte, but has not been reported up to now for asymmetric devices.

In the present study, large asymmetric activated carbon/MnO_2 cells have been assembled. After the presentation of the characteristics of each electrode materials, we report the excellent stability upon long-term cycling of such cells. Moreover, the use of a large capacitance device (380 F) built up from the assembly of more than 20 single cells is also reported, highlighting the potentiality of scaling up this technology.

2. Experimental

2.1. Activated carbon

Activated carbon was PICACTIF obtained from PICA Company. This carbon has a d_{50} of 10 μm, i.e. 50 wt.% of activated carbon have grain diameter below 10 μm, and a high specific surface area (2300 m^2 g^{-1}), thus indicating that the activation treatment led to a highly microporous material, suitable for ion adsorption, with high specific capacitance in organic-based electrolyte (95 F g^{-1}) [4]. Table 1 summarizes the main physical characteristics of the activated carbon.

2.2. Preparation of amorphous MnO_2 by coprecipitation technique (co-MnO_2)

MnO_2 powder was synthesized using a simple co-precipitation method [21,22,24]. All reactants were kept at 20 °C. $KMnO_4$ (99% purity) was firstly dissolved in deionized water to reach a concentration of 0.05 M. While stirring the solution, a 0.05 M $MnSO_4$ solution was added dropwise. The $KMnO_4$ solution was kept in an ultrasonic bath during $MnSO_4$ addition. The $KMnO_4$:$MnSO_4$ molar ratio was 2:3. A dark brown precipitate was immediately obtained according to:

$$2\,KMnO_4 + 3\,MnSO_4 + 2\,H_2O \rightarrow 5\,MnO_2\downarrow + K_2SO_4 + 2\,H_2SO_4 \quad (1)$$

The solution was then centrifuged at 9000 rpm and the precipitate was dried at 80 °C for 2 h under primary vacuum. Finally, the powder was annealed in air at 200 °C for 12 h. Five grams of powder were synthesized per batch. The large amount of MnO_2 (60 g) required for the fabrication of a hybrid prototype was obtained by mixing the powders of several batches, after checking their electrochemical properties.

2.3. Electrode elaboration

Composite electrodes were prepared by mixing the active material (MnO_2) in ethanol with acetylene black (Alfa Aesar, >99.9%, surface area = 80 m^2 g^{-1}), and polytetrafluoroethylene (PTFE) dried powders in the following weight ratios: 60/30/10. This composition was chosen, according to a previous study by Toupin et al. [24]. At least 15 wt.% carbon black is required to enhance the electronic conductivity of the positive electrode, since MnO_2 is poorly conductive. For the present study, a larger amount (30%) was used in order to decrease the ESR and thus to

Table 1
Physical characteristics of PICACTIF activated carbon

Specific surface area (BET) (m^2 g^{-1})	2310
Microporous volume (cm^3 g^{-1})	0.98
Mesoporous volume (cm^3 g^{-1})	0.68
Macroporous volume (cm^3 g^{-1})	0.65
Total porous volume (cm^3 g^{-1})	2.31

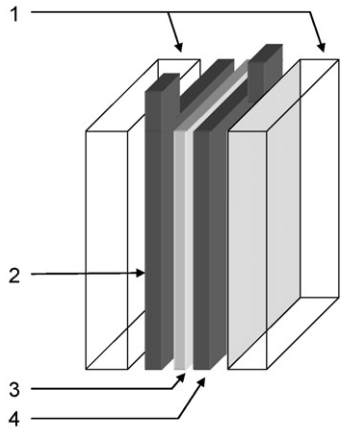

Fig. 1. Design of the hybrid supercapacitor: (1) PTFE supports, (2) positive MnO_2 composite electrode pressed on a stainless steel current collector, (3) glass fiber paper separator and (4) negative activated carbon composite electrode pressed on a stainless steel current collector.

improve the power density of the devices. The polymer binder content (10 wt.%) was chosen to provide a good mechanical integrity to the electrode, especially when preparing the thick films. This composition will have to be optimized for industrial prototypes. The mixture was heated at 60–80 °C to partially evaporate the solvent. The resulting black paste was then cold rolled into 100 μm thick films subsequently dried at 80 °C in air. Activated carbon electrodes were prepared using the same technique except with a mixture of 95% of active material and only 5% of PTFE.

Small individual cells were built using rectangular (Fig. 1) or disk-shaped electrodes (16 and 28 mm diameter). Each electrode has a stainless steel strip (0.5 cm × 2 cm) in order to facilitate electrical connection. The film thickness was adjusted by considering the specific charge storage capacity of each material in the appropriate voltage windows and by calculating the appropriate amount of active material needed in each electrode. Details of this calculation are given below. The load of active material in each electrode was varied from 10 to 40 mg cm^{-2} without any noticeable change in the performance. Both electrodes (positive and negative) were pressed at 900 MPa onto stainless steel grids to ensure a good electronic conductivity. As shown in Fig. 1, hybrid cells were fabricated by pressing both electrodes (activated carbon as the negative electrode and the positive MnO_2 electrode) between two PTFE supports, using a glass fiber paper as separator.

Electrochemical experiments were performed using a Solartron 1470 battery tester operated under Corrware II software (Scribner Associates). Rectangular-shaped electrodes were preferably used for single electrode tests. For such measurements, an Ag/AgCl (3 M NaCl) assembly and platinum gauze were used as reference and counter electrodes, respectively. In this study, all electrodes were tested in 0.1 M K_2SO_4. Single electrode tests and complete cell measurements were performed in 30 mL of electrolyte in a glass vial. All measurements were performed at room temperature.

The specific capacitance C (F g^{-1}) of a given electrode (activated carbon or MnO_2) was determined by integrating the cyclic voltammogram curve to obtain the corresponding voltammetric charge (Q_T). The voltammetric charge related to the presence of acetylene black (specific capacitance: 12 F g^{-1}) in the MnO_2 composite electrode was subtracted from the value of Q_T to calculate the charge only related to MnO_2 (Q) active material. Finally, Q was divided by the weight of the composite electrode (m), by considering the amount of active material in one electrode (x in %) and the width of the potential window (ΔE):

$$C = \frac{Q}{\Delta E\, x\, m} \tag{2}$$

Galvanostatic cycling measurements were performed between 0 and 2 V (or between 1 and 2 V) at various current densities (10–600 mA cm^{-2}). The equivalent series resistance (ESR) is measured by the current interrupt technique at each end of charge. In first approximation, the cell voltage V_{cell} can be described by the following equation:

$$V_{cell} = ESR \times I + \frac{Q}{C} \tag{3}$$

where C is the capacitance, Q the amount of charge stored at the electrode and I is the constant current used for the galvanostatic experiment. When the current is switched off, the cell voltage drops down to V'_{cell}, expressed as:

$$V'_{cell} = \frac{Q}{C} \tag{4}$$

In our case, V'_{cell} was measured 1 ms after the current was switched off. Combining Eqs. (3) and (4) gives the ESR value:

$$\mathrm{ESR} = \frac{V_{cell} - V'_{cell}}{I} \tag{5}$$

The measured ESR was measured at 1 kHz in electrochemical impedance spectroscopy. This technique allows determining the ESR variation upon cycling. Cell capacitance (C in F) is deduced from the slope of the discharge (dV/dt in V s^{-1}) curve by dividing the discharge current (I in A) by the slope:

$$C = \frac{I}{\mathrm{d}V/\mathrm{d}t} \tag{6}$$

2.4. Fabrication of large capacitance device

To demonstrate the scaling up potential of the hybrid device, larger cells were assembled through the stacking of several electrodes in parallel to increase the capacitance. A prismatic design was chosen for the device using a PVC casing ((L) 52 mm × (l) 49 mm × (h) 86 mm) and AISI 304 grids as current collectors. Stainless steel grids were first mechanically laminated down to 200 μm. Stainless steel pieces were then cut (Fig. 2a). The electrodes dimensions used to build-up the prototype were 60 mm × 43 mm. A strip of stainless steel (40 mm × 10 mm) free of electrode material was used to weld the whole series of current collectors.

The stainless steel current collectors were first polished with 180 grad SiC paper then covered with a carbon conductive paint-

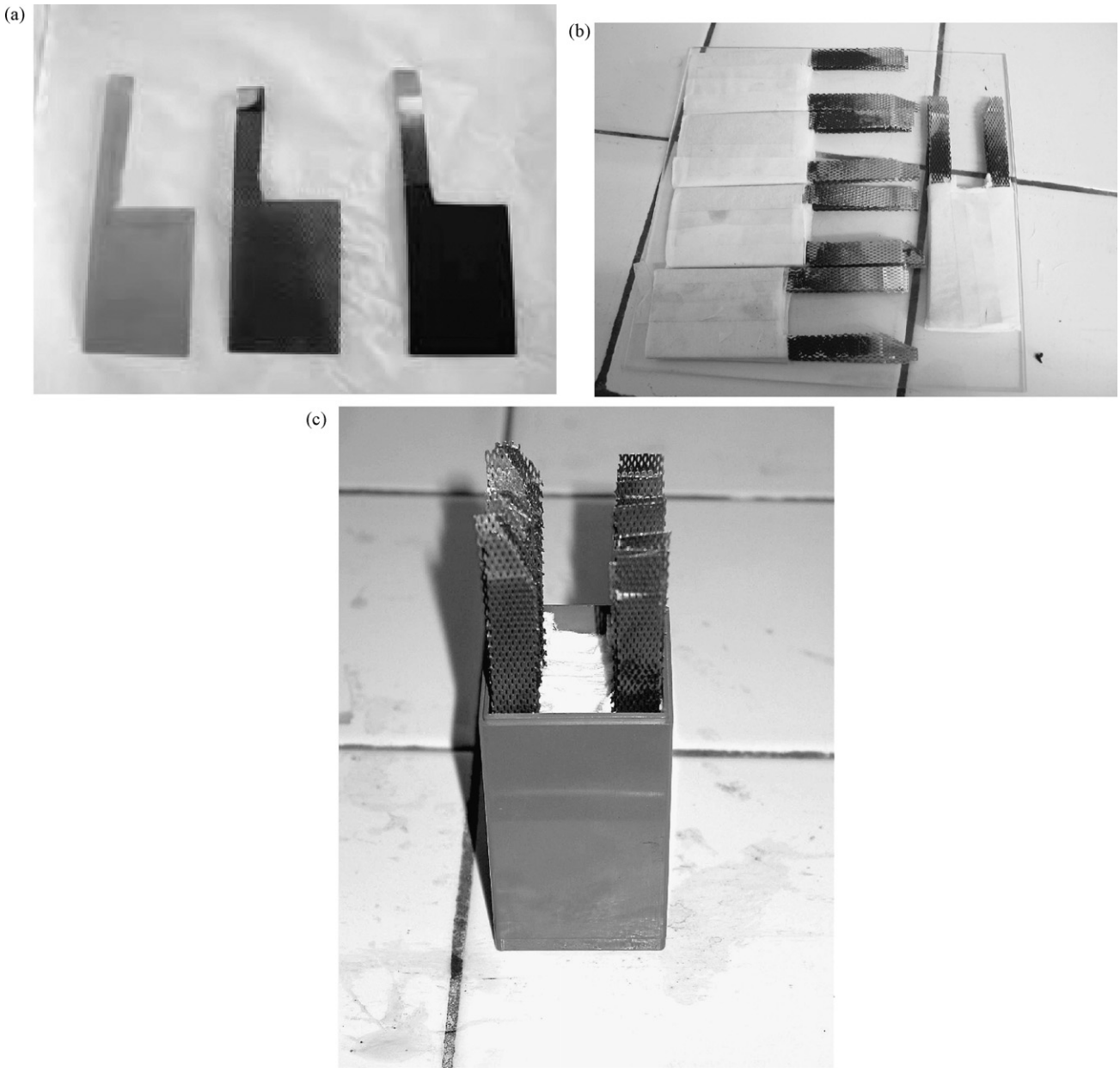

Fig. 2. (a) From left to right: AISI 304L stainless steel current collector, coated with conductive paint and co-laminated with the active material composite film, (b) 10-pack cells covered with a cellulosic paper separator and (c) large capacitance final device in the PVC casing prior to sealing.

ing (Fig. 2a) in order to lower the interface resistance between the current collector and the active material film. The weight ratio between the positive and negative electrode (electroactive materials) was adjusted at 1.65 ± 0.08. Painted current collectors were double-sided covered by the films of active material for an overall thickness of 400 μm (right side of Fig. 2a). Each electrode was wrapped in a cellulosic paper separator, 50 μm thick. The electrodes were assembled by stack of 10 units (Fig. 2b) and installed in the PVC casing (Fig. 2c). The vial was filled with 0.1 M K_2SO_4 outgased 15 min with N_2, prior to be sealed. The results presented in this study are related to a stack of 20 positive and 20 negative electrodes. It can be noted that this device was only built to evaluate the feasibility of stacking unit cells in parallel and the corresponding characteristics: capacitance and resistance. This device cannot be considered as a prototype since the shape of current collectors, the amount of electrolyte, the electrode thickness, the casing and the packaging were not optimized. Electrochemical tests were performed in the same manner as for small single cells.

3. Results and discussion

3.1. Single cell characteristics

A typical cyclic voltamogramm of the MnO_2 positive electrode is depicted in Fig. 3a. The oxide electrode can be cycled between −0.1 and +1.0 V versus Ag/AgCl, but in order to avoid side reactions, such as manganese dissolution at low potential

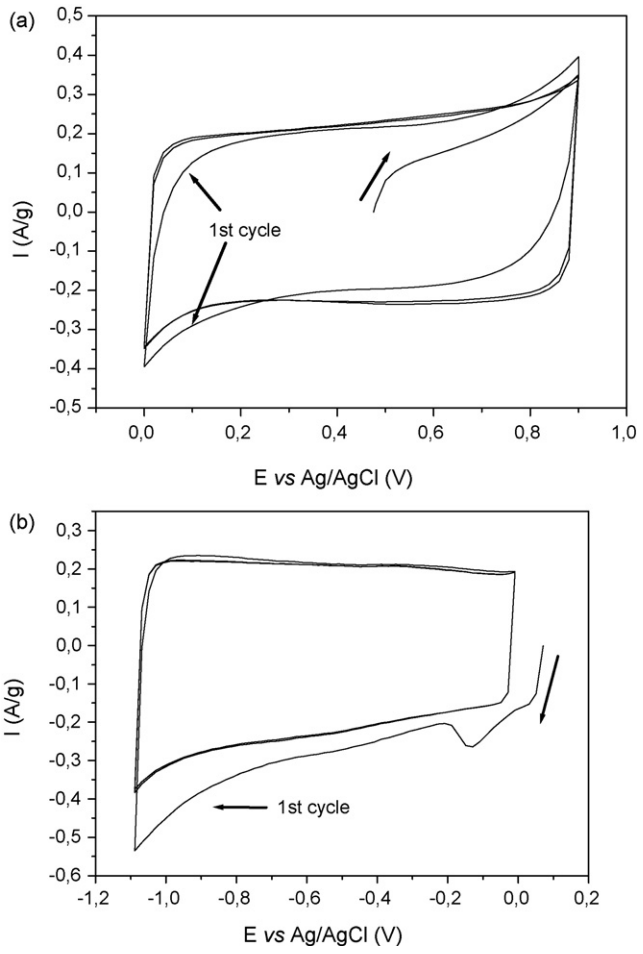

Fig. 3. Cyclic voltamogramm of (a) MnO_2 electrode and (b) activated carbon (AC) electrode; scan rate = 2 mV s^{-1}.

or oxygen evolution reaction at high potential [31] the useful electrochemical window should be kept between 0 and 0.9 V versus Ag/AgCl. For the activated carbon (AC) negative electrode, the potential window can be extended to more negative potential, i.e. −1.3 V versus Ag/AgCl (Fig. 3b), but a noticeable hydrogen evolution reaction occurs below this potential. Moreover, even if the upper potential limit can be extended to 0.4 V versus Ag/AgCl for the AC electrode, it should be kept at 0 V to have a complementary and adjusted potential window for both positive and negative electrodes with the weight ratio we used. To provide a 2 V cell voltage, a targeted potential window from −1.1 to 0 V versus Ag/AgCl was used for the activated carbon negative electrode, and from 0 to 0.9 V for the MnO_2 positive electrode.

The specific capacitance of each electrode of the hybrid cell was evaluated by cyclic voltammetry (CV). The specific capacitance C (F g^{-1}) of a given MnO_2 electrode was determined by integrating the CV curve to obtain the voltammetric charge of the positive electrode (Q_+). The voltammetric charge relative to the presence of acetylene black (specific capacitance: 12 F g^{-1}) in the composite electrode was subtracted from the value of Q_+ to extract the charge relative only to the active material (Q_{MnO_2}). Finally, the specific capacitance was calculated by dividing Q_{MnO_2} by the weight of active material (m_{MnO_2}) in the composite positive electrode (60%) and by the effective potential window (ΔE_{MnO_2}) used to perform the CV:

$$C_{MnO_2} = \frac{Q_{MnO_2}}{\Delta E_{MnO_2}\, m_{MnO_2}} \tag{7}$$

The same calculation was performed to determine the specific capacitance C_{AC} of activated carbon negative electrode.

$$C_{AC} = \frac{Q_{AC}}{\Delta E_{AC}\, m_{AC}} \tag{8}$$

where Q_{AC} is the voltammetric charge related to the weight of activated carbon (deduced from Q_- the voltammetric charge of the negative electrode, Fig. 3b), m_{AC} the weight of activated carbon in the electrode and ΔE_{AC} is the working potential window used for the CV.

According to Eqs. (7) and (8), the specific capacitance of the positive electrode is 72 F g^{-1} resulting from 120 F g^{-1} for MnO_2, calculated for a 0–0.9 V potential window. This value is in good agreement with those reported by Toupin et al. [24] for manganese dioxide powder synthesized with the same coprecipitation technique and heat-treated at 200 °C. According to the amount of MnO_2 in the composite electrode (60 wt.%), the voltammetric charge of the positive electrode is 65 C g^{-1} (18 mAh g^{-1}).

For the calculation of the activated carbon specific capacitance, a −1.1 to 0 V potential window was used (Fig. 3b). A value of 95 F g^{-1} was determined for the complete negative electrode, i.e. 100 F per gram of activated carbon. Thus, the voltammetric charge of the composite negative electrode is 105 C g^{-1} (29.2 mAh g^{-1}). Subsequently, to ensure the charge balance of the hybrid cell, the weight ratio between the negative and the positive electrodes was $k = m_+/m_- = 1.65 \pm 0.08$.

The typical CV of a hybrid cell is depicted in Fig. 4a. Galvanostatic plots (constant current charge/discharge cycling) for each electrode are shown in Fig. 4b. The hybrid device was cycled between 0 and 2 V with a very good reversibility in this potential window. As can be seen in Fig. 4b, the electrochemical windows slightly varied from those expected for both electrodes.

The MnO_2 electrode potential increases from 0 to 0.8 V upon charging while that of the activated carbon electrode varied from 0 to −1.2 V. These electrochemical windows slightly vary from one cell to another (±100 mV on each side during the first 100 cycles) but without noticeable influence on the performance of the hybrid supercapacitor. More than 20 cells were assembled with the same design and showed very reproducible values of the specific capacitance (21 ± 2 F g^{-1}, related to the sum of the positive and negative composite electrode weights) when cycled at room temperature. The theoretical capacitance (expressed in F) of the hybrid cell, C'_H, can be calculated according to:

$$C'_H = \frac{C' + C'_-}{C'_+ + C'_-} \tag{9}$$

where C'_+ and C'_- are the capacitance of the positive and negative electrodes (expressed in F), respectively. Relative to the weight

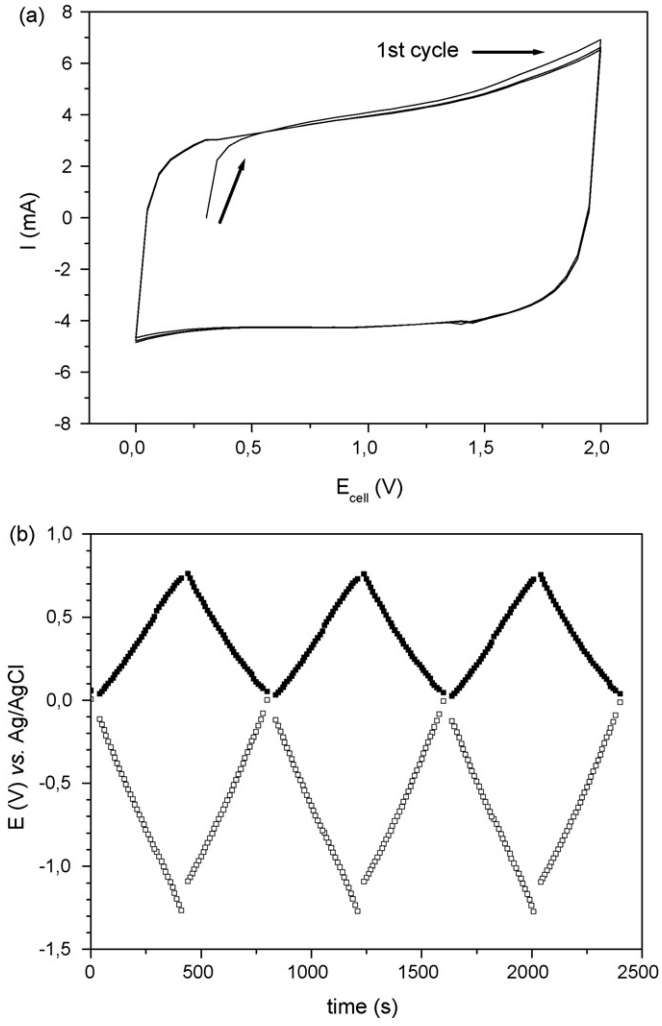

Fig. 4. (a) Cyclic voltammogram of the hybrid AC–MnO_2 cell (scan rate = 2 mV s^{-1}) and (b) corresponding galvanostatic plots for each electrode (charge/discharge current 2.5 mA cm^{-2}).

ratio of active materials, Eq. (9) translates into:

$$C_H = \frac{C_+ C_-}{C_- + kC_+} \times \frac{k}{1+k} \quad (F\,g^{-1}) \tag{10}$$

where C_+, C_- and C_H are expressed in F g^{-1} and $k = m_+/m_-$ is the weight ratio, i.e. 1.65. Since the specific capacitance of the positive electrode is $C_+ = 72$ F g^{-1} and the specific capacitance of the negative electrode is $C_- = 95$ F g^{-1}, and from Eq. (10), the value of the specific capacitance of the hybrid cell is found to be equal to 20 F g^{-1} (related to the sum of both electrode weights). This value agrees very well with the measured capacitance (21 ± 2 F g^{-1}). Such values of capacitance compare well with those of organic-based carbon/carbon cells. For example, the cell capacitance determined from the recent work of Portet et al. [6] gives a reproducible value of 22.6 F g^{-1} between 0 and 2.3 V in 1.5 M $N(C_2H_5)_4BF_4$ in acetonitrile. The maximum power and energy densities of our cells can also be calculated and compared to those reported by Portet et al. [6]. The maximum power density is given by Eq. (11), where V is the cell voltage and m the total weight of both composite electrodes, i.e. $m_+ + m_-$:

$$P_{max} = \frac{V^2}{4(ESR)\,m} \quad (W\,kg^{-1}) \tag{11}$$

The maximum energy density is obtained from the capacitance of the cell:

$$E_{max} = \frac{(1/2)\,C\,V^2}{3600\,m} = \frac{(1/2)\,C_H\,V^2}{3600} \quad (Wh\,kg^{-1}) \tag{12}$$

Subsequently, the maximum energy density of the aqueous system (average value of 11.7 Wh kg^{-1} of total electrode materials) is 72% that of the organic one (16.2 Wh kg^{-1} of total electrode materials), without needs of any anhydrous salt and special manufacturing water-free atmosphere. Moreover, the aqueous hybrid cell, alike the organic-based carbon/carbon supercapacitors, can also tolerate punctual overcharge up to 2.7 V without any noticeable influence on the capacitance value [29].

3.2. Long-term cycling

Previous studies have shown that such hybrid devices can undergo more than 20,000 cycles in a mild aqueous electrolyte with, however, a noticeable fade of energy density [31]. It indeed faded down to only 77% of its initial energy density after 23,000 cycles even when the maximum cell voltage was as low as 1.5 V. In that case, the post-mortem analysis of the electrodes has shown brown spots on stainless steel current collectors. To prevent any corrosion, suspecting that it could arise from the presence of dissolved oxygen in the aqueous electrolyte, a 15-min nitrogen bubbling was performed prior to sealing of the cell. As a comparison, an identical cell was assembled with the same procedure but without any N_2 bubbling. Both cells were cycled at constant current densities of 30 mA cm^{-2} (1.5 A g^{-1}) between 0 and 2 V. The initial capacitances of the hybrid supercapacitors were 23 and 21 F g^{-1} for the standard cell and the outgased one, respectively.

The small differences in the inital capacitance and resistance values are due to small weight and thickness differences of the electrodes. The resistance and capacitance of both cells were recorded during several thousand cycles (Fig. 5). The standard cell assembled without outgasing with N_2 shows a monotonous decrease of capacitance upon cycling, which reached only 53% of the initial value after 50,000 cycles. Meanwhile, the internal resistance of the standard device increased by 167%. On the contrary, the cell outgased with N_2 shows a very good stability over 60,000 cycles, with 93% of its initial value when the cell was stopped and the resistance only increased by 28%.

The improvement of the stability of the capacitor in the absence of oxygen is presumably related to the limitation of the corrosion of the current collectors. Indeed, the role of dissolved oxygen was recently pointed out in the crevice corrosion of AISI 304L stainless steel [36]. Stainless steels are particularly sensitive to this corrosion mechanism, for which oxygen reduction initially takes place on the whole metallic surface. For the negative stainless steel current collector immersed in aqueous K_2SO_4 neutral electrolyte, the onset of oxygen reduc-

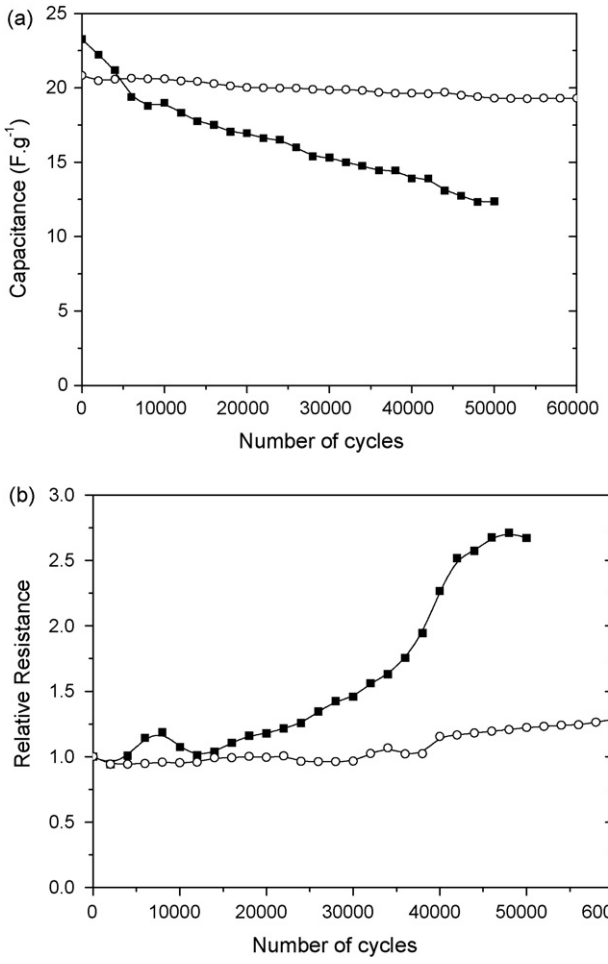

Fig. 5. (a) Capacitance of a hybrid AC–MnO_2 cell without (black squares) and with (white dots) N_2 bubbling (charge/discharge current = 30 mA cm^{-2} between 0 and 2 V, one charge/discharge cycle during 56 s at the beginning of the test) and (b) evolution of the relative resistance $\Delta R/R_{ini}$ of the cell without (black squares) and with (white dots) N_2 bubbling.

tion was observed at −0.6 V versus Ag/AgCl, consistent with literature data [36]. Some parts of the current collector of the negative electrode of the capacitor are in intimate contact with the electrolyte, while limited amounts of electrolyte are trapped between the stainless steel grid and the composite electrode film. Subsequently, electrolyte convection within the "hidden" surfaces is very limited and oxygen is rapidly locally depleted. The difference between oxygen concentrations in the two kinds of surfaces leads to the formation of a "concentration cell" [37]. Consequently, metal oxidation occurs within the confined areas, leading to the dissolution of metallic ions (iron, chromium, nickel) which accumulate in these areas and which are electrically balanced by electrolytic migration of sulphate ions. This phenomenon is amplified on stainless steels since oxygen depletion inhibits in the confined areas the formation of a passive layer at the metal surface. The hydrolysis of highly concentrated metallic sulphate solutions induces a subsequent drastic decrease of pH, which in turn accelerates the corrosion process. As a result, the oxygen-depleted area is submitted to intense corrosion, with subsequent localized loss of electrical conductivity (resistance increases upon cycling) and more difficult access of

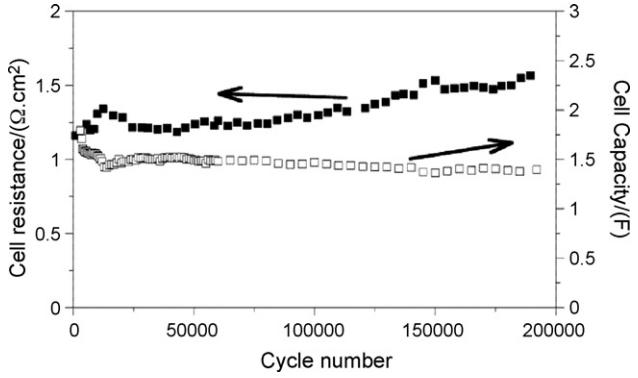

Fig. 6. Capacitance (open squares) and resistance (black squares) of a hybrid AC–MnO_2 cell. Charge/discharge current 40 mA cm^{-2} between 0 and 2 V, one charge/discharge cycle during 130 s at the beginning of the test.

alkaline ions to the surface of the composite electrode due to corrosion products (capacity decreases upon cycling). Indeed these two phenomena are observed in the case on non-outgased electrolyte solutions.

When the negative stainless steel current collector is immersed in aqueous K_2SO_4 neutral electrolyte, the onset of oxygen reduction still occurs at −0.6 V versus Ag/AgCl but the related cathodic current density is 5–10 times lower than for non-outgased electrolyte solution. Subsequently, the formation of oxygen "concentration cell" is slowed down, thus limiting crevice corrosion phenomena, which will however still occur after a longer time.

The presence of Mn^{2+} ions or the use of excessive positive potential on the MnO_2 side together with significant concentrations of dissolved oxygen can also be partly responsible for corrosion phenomena of the stainless steel current collectors.

Following these results, additional laboratory cells were assembled and tested for long-term cycling, for over more than 195,000 cycles, thus demonstrating the excellent stability of the hybrid cell (Fig. 6). The capacitance faded by 12.5% over 195,000 cycles. This represents a substantial improvement relative to the tests performed on other hybrid systems involving pseudo-capacitive electrodes previously described in literature that were carried out for only few hundred or thousand cycles [20,29–33,38,39]. For example, the Fe_3O_4/MnO_2 hybrid supercapacitor designed by our group [20] shows a drastic capacitance fading (12.5%) after only 2000 cycles. As another example, a carbon/polymethylthiophene hybrid capacitor [39] showed good performance but with continuous decrease of the capacity upon cycling (up to 40% loss after 10,000 cycles).

The ESR determined at 1 kHz (1.3 Ω cm^2) is slighlty higher than the usual value measured for an organic device with optimized current collectors (<1 Ω cm^2) [4,6]. Nonetheless, there is room for improvement on the ESR value for the aqueous device, since neither the current collector nor the composite electrode composition have been optimized during this work. The ESR of this hybrid aqueous system increased by 27% during the first 195,000 cycles. This limited ESR change upon cycling is also a promising result when compared to other asymmetric systems [30], demonstrating the attractive performance of the C/MnO_2 supercapacitor presented here.

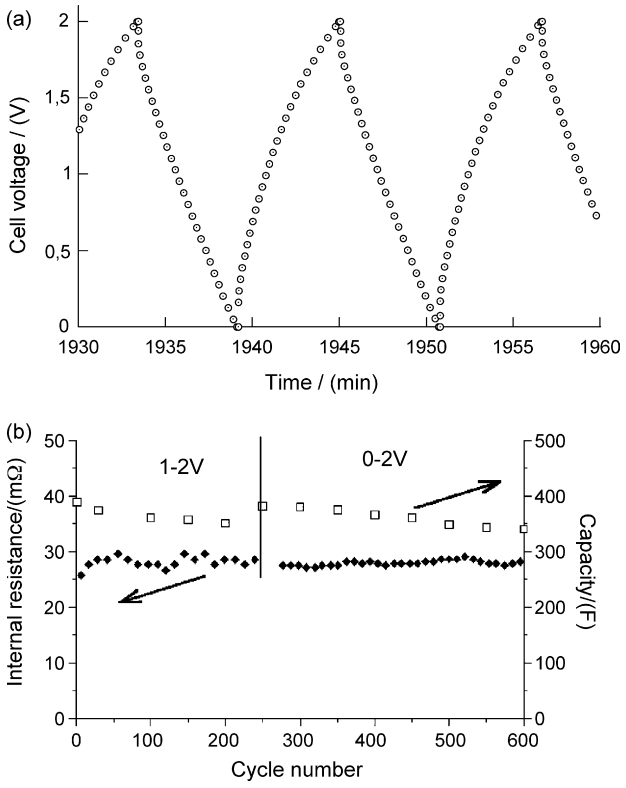

Fig. 7. Characterization of a 380-F hybrid supercapacitor demonstrator: (a) representative galvanostatic cycles (constant current = 2 A) and (b) variation of capacity and resistance with cycle number.

3.3. Large capacitance stacks

Cells built by stacking 40 electrodes (20 positive and 20 negative) were prepared according to the procedure described in Section 2. Fig. 7a shows the charge/discharge plots for this stack under a constant current of 2 A, which is the upper current limit for our galvanostat. The capacitance of the device is 380 F (Fig. 7b) and fits well with the amount of MnO_2 and activated carbon used to prepare the electrodes. The ESR is higher than expected, probably due to unoptimized separator thickness: four cellulosic paper sheets were used to separate each cell to avoid short-circuiting between them. The device was cycled over more than 600 cycles without any significant fade in the electrochemical performances. To the best of our knowledge, this is the first report for the fabrication of such large cells (380 F) using the hybrid carbon/MnO_2 technology in mild aqueous electrolyte. These first results are obviously encouraging and future works will be aimed at the fabrication of optimized prototypes.

4. Conclusion

We have reported here the long-term electrochemical behavior of a hybrid capacitor using a negative activated carbon electrode and a positive MnO_2 composite electrode, cycled in a mild aqueous electrolyte (0.1 M K_2SO_4). This capacitor shows very attractive energy storage characteristic for a 2 V supercapacitor in aqueous media. An improved cycle life was achieved in O_2-free electrolyte, which minimized the corrosion of stainless steel current collectors. Indeed, outgased electrolyte results in the limitation of crevice corrosion of the negative current collector. More than 195,000 cycles were achieved with remarkable capacitance retention, capacitance fade limited to 12.5% and good resistance stability (+27% in 195,000 cycles). These results led to specific energy and specific power of 10 Wh kg^{-1} and 16 kW kg^{-1}, respectively, after 195,000 cycles. Moreover, we have shown the feasibility of manufacturing large packs (2 V–380 F) by stacking several single hybrid cells, with excellent performance reproducibility. Stable performance were demonstrated over 600 cycles using our large capacitance device. Even though some technological optimizations are needed to improve the device. This study highlights the opportunity to develop large cells using these design and fabrication approaches, with non-toxic and safer components compared to the usual organic-based devices.

Acknowledgements

The authors would like to thank Dr. Emilie Machefaux and Dr. Dominique Guyomard (LCS-IMN, Nantes, France) for their help with the long-term cycling measurements. Prof. René Le Gall is acknowledged for helpful discussion on corrosion phenomena. The financial support of MENRT/DGA/CNRS (CAPRYS project PR6-2, ACI Energie 2003) is greatly acknowledged. The French "Ministère des Affaires Etrangères" and "Ministère des Relations Internationales du Québec" are also greatly acknowledged for partially supporting this work. The authors would like to thanks the PICA Company for the activated carbon samples.

References

[1] B.E. Conway, Electrochemical Supercapacitors Scientific Fundamentals and Technological Applications, Kluwer Academic/Plenum Press, New York, 1999.
[2] A. Burke, J. Power Sources 91 (2000) 37–50.
[3] M. Winter, R.J. Brodd, Chem. Rev. 104 (2004) 4245–4269.
[4] P.L. Taberna, P. Simon, J.F. Fauvarque, J. Electrochem. Soc. 150 (2003) A292–A300.
[5] M. Toupin, D. Bélanger, I.R. Hill, D. Quinn, J. Power Sources 140 (2005) 203–210.
[6] C. Portet, P.L. Taberna, P. Simon, E. Flahaut, J. Electrochem. Soc. 153 (2006) A649–A653.
[7] E. Lust, A. Janes, M. Arulepp, J. Electroanal. Chem. 562 (2004) 33–42.
[8] P. Guillemet, Y. Scudeller, T. Brousse, J. Power Sources 157 (2006) 630–640.
[9] J. Schiffer, D. Linzen, D. Uwe Sauer, J. Power Sources 160 (2006) 765–772.
[10] S. Ardizzone, G. Fregonara, S. Trasatti, Electrochim. Acta 35 (1990) 263–267.
[11] H. Kim, B.N. Popov, J. Power Sources 104 (2002) 52–61.
[12] K.H. Chang, C.C. Hu, Electrochem. Solid-State Lett. 7 (2004) A466–A469.
[13] P. Soudan, J. Gaudet, D. Guay, D. Bélanger, R. Schulz, Chem. Mater. 14 (2002) 1210–1215.
[14] A. Rudge, J. Davey, I. Raistrick, S. Gottesfeld, J.P. Ferraris, J. Power Sources 47 (1994) 89–107.
[15] F. Fusalba, N. El Mehdi, L. Breau, D. Bélanger, Chem. Mater. 11 (1999) 2743–2753.
[16] E. Naudin, H.A. Ho, S. Branchaud, L. Breau, D. Bélanger, J. Phys. Chem. B 106 (2002) 10585–10593.

[17] N.L. Wu, S.Y. Wang, C.Y. Han, D.S. Wu, L.R. Shiue, J. Power Sources 113 (2003) 173–178.
[18] N.L. Wu, Mater. Chem. Phys. 75 (2002) 6–11.
[19] S.Y. Wang, N.L. Wu, J. Appl. Electrochem. 33 (2003) 345–348.
[20] T. Brousse, D. Bélanger, Electrochem. Solid-State Lett. 6 (2003) A244–A248.
[21] H.Y. Lee, J.B. Goodenough, J. Solid State Chem. 144 (1999) 220–223.
[22] H.Y. Lee, V. Manivannan, J.B. Goodenough, C. R. Acad. Sci. II C (1999) 565–577.
[23] C.C. Hu, T.W. Tsou, Electrochim. Acta 47 (2002) 3523–3532.
[24] M. Toupin, T. Brousse, D. Bélanger, Chem. Mater. 14 (2002) 3946–3952.
[25] Y.U. Jeong, A. Manthiram, J. Electrochem. Soc. 149 (2002) A1419–A1422.
[26] H. Kim, B.N. Popov, J. Electrochem. Soc. 150 (2003) D56–D62.
[27] S.C. Pang, M.A. Anderson, T.W. Chapman, J. Electrochem. Soc. 147 (2000) 444–450.
[28] T. Brousse, M. Toupin, R. Dugas, L. Athouël, O. Crosnier, D. Bélanger, J. Electrochem. Soc. 153 (2006) A2171–A2180.
[29] T. Cottineau, M. Toupin, T. Delahaye, T. Brousse, D. Bélanger, Appl. Phys. A: Mater. 82 (2006) 599–606.
[30] M.S. Hong, S.H. Lee, S.W. Kim, Electrochem. Solid-State Lett. 5 (2002) A227–A230.
[31] T. Brousse, M. Toupin, D. Bélanger, J. Electrochem. Soc. 151 (2004) A614–A622.
[32] V. Khomenko, E. Raymundo-Piñero, F. Béguin, J. Power Sources 153 (2006) 183–190.
[33] V. Khomenko, E. Raymundo-Piñero, E. Frackowiak, F. Béguin, Appl. Phys. A: Mater. 82 (2006) 567–573.
[34] M. Toupin, T. Brousse, D. Bélanger, Chem. Mater. 16 (2004) 3184–3190.
[35] W.G. Pell, B.E. Conway, J. Power Sources 136 (2004) 334–345.
[36] Y.P. Kim, M. Fregonese, H. Mazille, D. Feron, G. Santarini, Corros. Sci. 48 (2006) 3945–3959.
[37] L.D. Landolt, Traité des matériaux, vol. 12, Corrosion et chimie de surfaces des métaux, première édition, Presse polytechniques et universitaires Romandes, Lausanne, 1993, pp. 260–266.
[38] Y.-G. Wang, Y.-Y. Xia, J. Electrochem. Soc. 153 (2006) A450–A454.
[39] A. Di Fabio, A. Giorgi, M. Mastragostino, F. Soavi, J. Electrochem. Soc. 148 (2001) A845–A850.